POLITECNICO
MILANO 1863

SCUOLA DI INGEGNERIA INDUSTRIALE
E DELL'INFORMAZIONE

IN-PLANE FINITE ELEMENT MODEL OF A BIKE FRAME

Department of Mechanical Engineering
Course of Dynamics of Mechanical Systems

Elisa Rita Rosanò 991950
Erika De Bardi 987096

Professor:
Prof. Alberto Zasso
Ing. Giulia Pomaranzi

Academic year:
2023-2024

Abstract: In the "continuum approach" the vibration of continuous systems is described by analytical models that result in Partial Differential Equations (PDE). The solution to the problem of computing the natural frequencies and the corresponding mode shapes can be found only in a limited number of cases, which correspond to specific boundary conditions. In order to solve the more general case, the only possibility is to make use of numerical methods.The most popular and versatile one is the Finite Element Method (FEM) that will be used in the present analysis in order to characterise a bike frame.

1. SYSTEM DESCRIPTION

The physical structure under analysis is a road bike, specifically its frame (Figure 1). The frame's material is aluminium being characterised by the following properties: $\rho = 2700\frac{Kg}{m}$, $E = 7 * 10^7 \frac{N}{m^2}$. All beams have a tubular cross section.

Figure 1: Road bike: physical system.

A simplified in-plane model for the bike frame, suitable for the FE discretisation, is presented below in Figure 2. The horizontal displacement of point C is prevented. Moreover, the lumped masses at points A, B, C, F represent the wheels, the crankset, the handlebar.

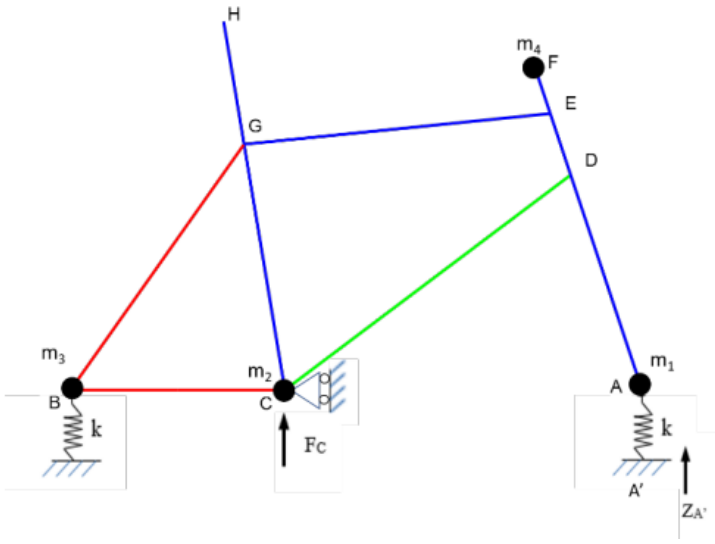

Figure 2: Road bike: FE model.

The system is analysed in the frequency range 0-200 Hz, therefore $\Omega_{max} = 200Hz$.

2. MESH GENERATION

In order to generate the appropriate mesh, 2 different criteria are present:

1. If there is a geometrical or material discontinuity, a node is placed at the interface. It can be noted that, if the material properties are uniform within the beam, not having further geometrical discontinuity, a second criteria must be applied in order to identify which are the proper nodes;
2. As a matter of fact, the element behaviour within 2 nodes is described by the shape functions, which are coincident with the static deformation of the system. Each elements must behave in a static condition,this means that the element must be short enough (KEY POINT).

Thus, to ensure that each beam element used to discretize the analyzed structure works in the quasi-static region, for assigned geometry of the beam cross-section and material properties, the length of any beam FE shall not exceed a certain limit value, which depends on the maximum frequency Ω_{max} of the analysis. The maximum admitted length was computed for each set of mass per unit length (m) and bending stiffness (EJ) as shown in Table 1.

	Beam	**m** $[\frac{Kg}{m}]$	**EJ** $[N \cdot m^2]$	L_{max} **[m]**
1	Red	0.1612	$1.891 \cdot 10^2$	0.3667
2	Blue	0.3381	$1.1727 \cdot 10^3$	0.4646
3	Green	1.0073	$7.3855 \cdot 10^3$	0.5799

Table 1: Properties and maximum length of each portion of the structure.

The maximum length has been computed as follows since each FE can be considered as a **simply supported beam**:

$$L_{max} = \sqrt{\frac{\pi^2}{2 \cdot \Omega_{max}} \sqrt{\frac{EJ}{m}}} \tag{1}$$

By doing that, the behaviour of the elements in the frequency range of interest is considered rigid, therefore it makes sense to describe the behaviour of the elements with shape functions representative

of their static behaviour.

As a first attempt the nodes were placed in the positions marked as A, B, C, D, E, F, G, H (Figure 1) but, after computing the maximum length, it was seen that some beams didn't comply with the required length and thus, with the first natural frequency condition on each element $w_{1,k}$, which must be much higher than the maximum frequency we expect:

$$\omega_{1,k} = \eta * \Omega_{max} \tag{2}$$

where $\eta = 2$ is the safety coefficient. Due to this, 5 more nodes (5, 7, 8, 11 and 12) have been added.

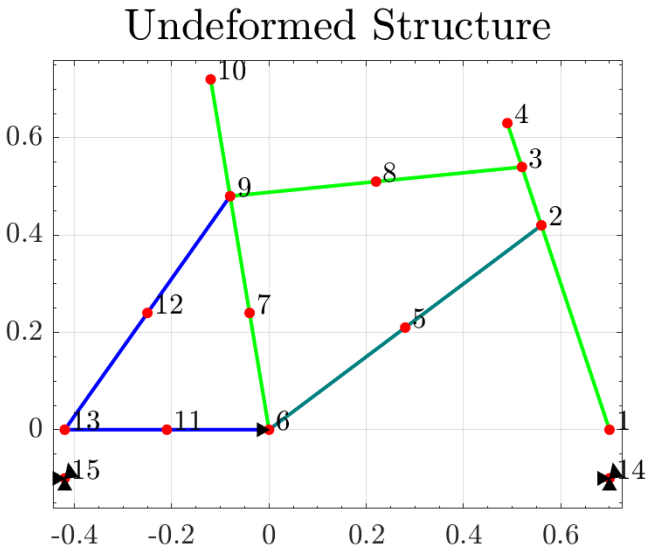

Figure 3: Undeformed structure.

Moreover, to take into account that the internal springs, representing the bike tyres, will be subjected to ground imposed displacements, nodes 14 and 15 have been included in the FE model. Their ordinates have been chosen arbitrarily since they are both connected to node 13 and node 1 with a spring and we are interested in their varied configuration with respect to the stable equilibrium position.

3. IDENTIFICATION OF NATURAL FREQUENCIES AND MODE SHAPES

After the mesh generation, the mass matrix and stiffness matrix are implemented adding concentrated stiffness and lumped masses. This passage has been performed summing up values of concentrated parameters with those present in assembled matrices referring to the node and direction of application. Note that the internal springs introduction consists in an easy procedure since in both cases the springs are aligned with the vertical direction coherent with the global reference frame.
Then, those matrices have been partitioned through the use of the Matlab code provided, result in the following form:

$$[M] = \begin{bmatrix} [M_{FF}] & [M_{FC}] \\ [M_{CF}] & [M_{CC}] \end{bmatrix}$$

$$[K] = \begin{bmatrix} [K_{FF}] & [K_{FC}] \\ [K_{CF}] & [K_{CC}] \end{bmatrix}$$

where FF comprises the free inertia/stiffness degrees of freedoms (DOFs) seen by the free DOFs, FC the constrained inertia/stiffness DOFs seen by the free DOFs, CF the free inertia/stiffness DOFs seen by the constrained DOFs and CC the constrained inertia/stiffness DOFs seen by the constrained DOFs.

Focusing on the FF sub matrices, through the results obtained solving the following eigenvalue problem:

$$\left(\omega^2 [I] - [M_{FF}]^{-1} [K_{FF}]\right) X = 0 \tag{3}$$

the natural frequencies can be computed as follows:

$$f_i = \frac{\omega_i}{2\pi} \tag{4}$$

Thus, also the mode shapes, up to the 4^{th} mode, are determined and shown in the figure below:

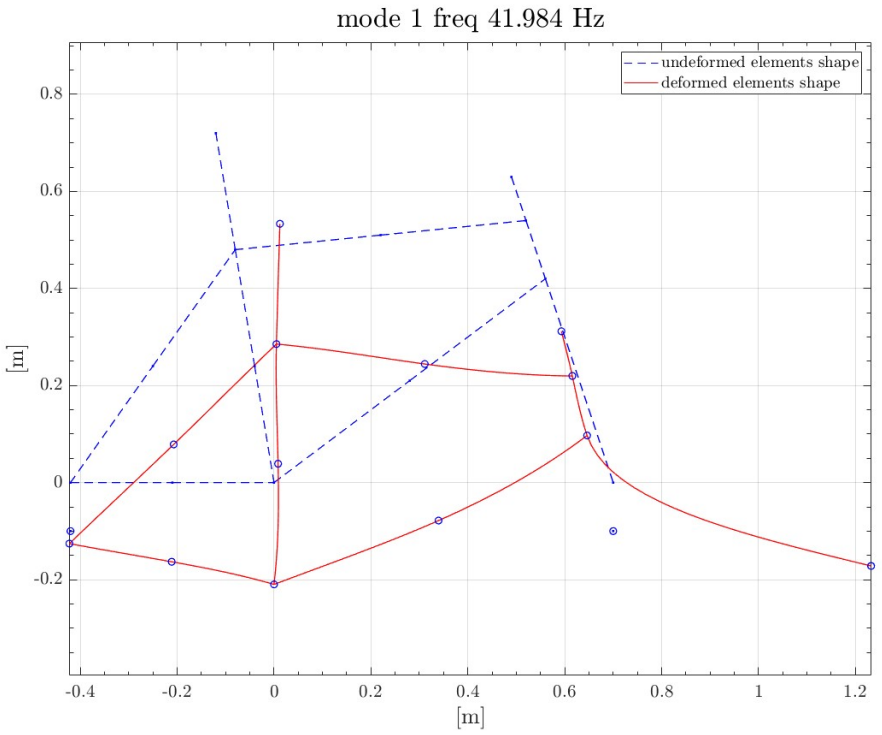

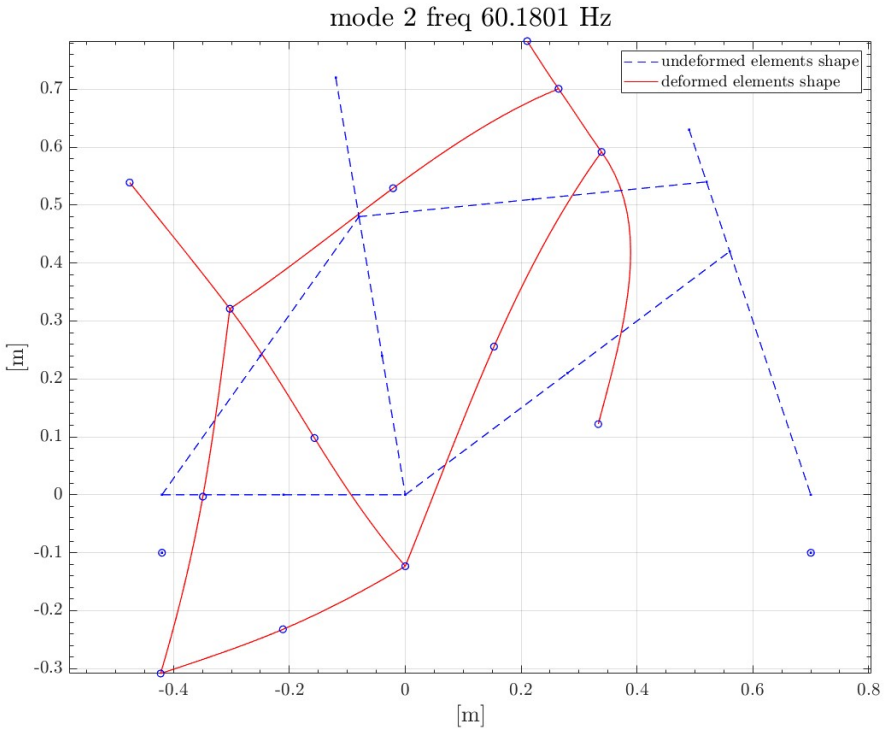

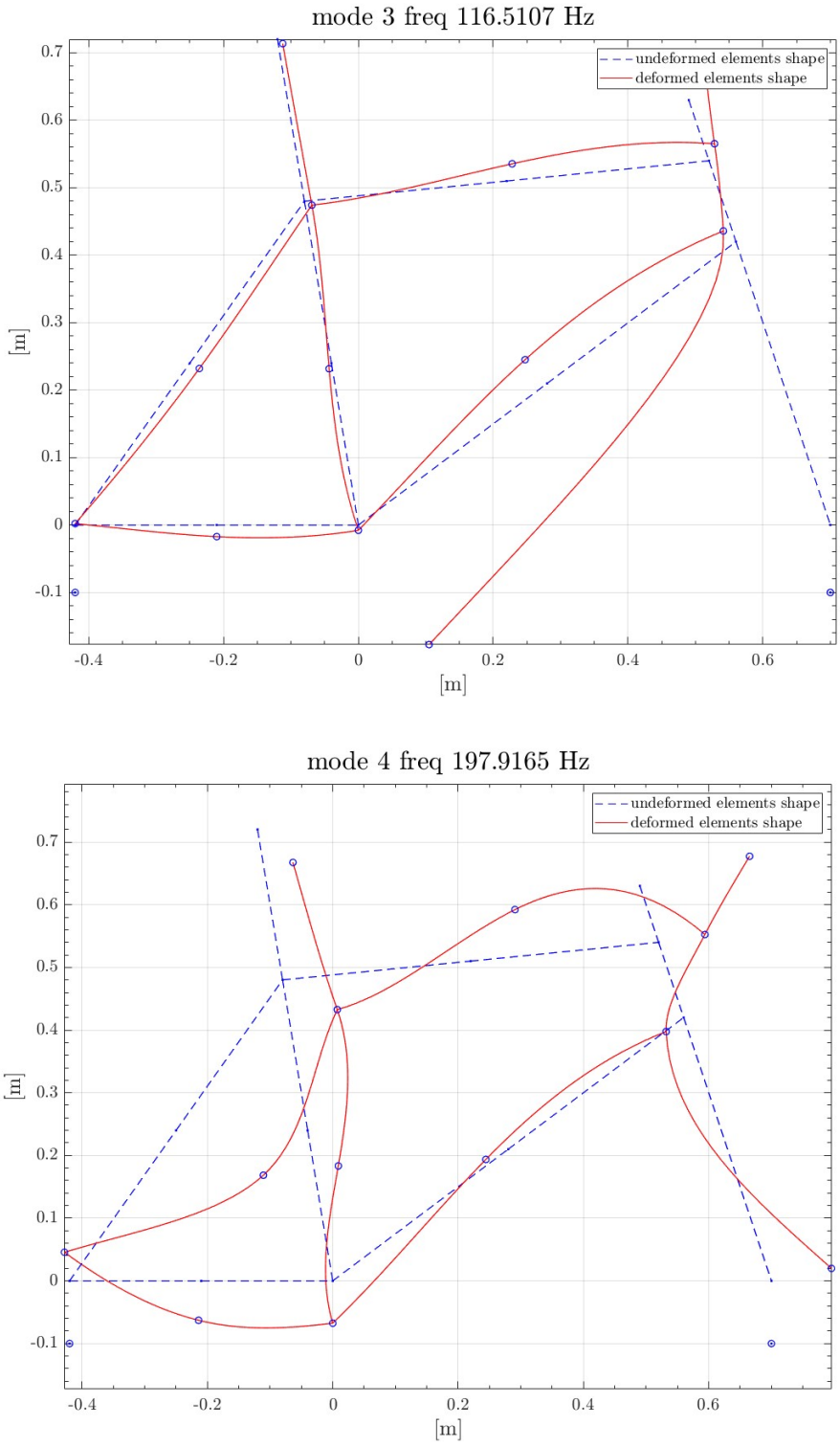

Figure 4: Vibration mode shapes up to the 4^{th} (scale factor = 2).

Since the mode shapes do not get the information about the amplitude, a **scale factor** is required in input. Everything is described as variation with respect to the reference configuration, thus those shapes are not representative of the real amplitude of the response but the relative displacements are correct.

4. DAMPING MATRIX

No lumped damping elements are present in the structure, despite this the bike frame is endowed by a certain amount of structural damping; therefore, in order to model this, the damping matrix is defined by means of the proportional damping assumption (Rayleigh's method):

$$[C] = \alpha\,[M] + \beta\,[K] \tag{5}$$

From the data of the problem we already know that $\alpha = 6s^{-1}$ and $\beta = 1 \cdot 10^{-5}s$.

When instead they are not directly provided, assuming that the damping ratios ξ_i have been identified by means of proper modal parameters identification techniques starting from an experimental modal analysis, the coefficients α and β necessary to compute the damping matrix can be identified as follows:

$$\xi_i = \frac{\alpha}{2\omega_i} + \frac{\beta\omega_i}{2} \tag{6}$$

$$[A]\begin{bmatrix}\alpha\\ \beta\end{bmatrix} = \underline{B} \tag{7}$$

$$\begin{bmatrix}\alpha\\ \beta\end{bmatrix} = [A]^{-1}\underline{B} \tag{8}$$

$$\text{where } [A] = \begin{bmatrix} \frac{1}{2\omega_1} & \frac{\omega_1}{2} \\ \vdots & \vdots \\ \frac{1}{2\omega_i} & \frac{\omega_i}{2} \\ \vdots & \vdots \\ \frac{1}{2\omega_N} & \frac{\omega_N}{2} \end{bmatrix} \text{ and } \underline{B} = \begin{bmatrix} \xi_1 \\ \vdots \\ \xi_i \\ \vdots \\ \xi_N \end{bmatrix}$$

5. FREQUENCY RESPONSE FUNCTIONS

Considering a **vertical input force in node C (F_C)** that varies in the 0-200 Hz frequency range and setting 0.01 Hz as frequency resolution, it has been calculated the Frequency Response Functions (FRF) that correlates the aforementioned force to the following outputs:

- Vertical displacement and vertical acceleration of node F, horizontal displacement and horizontal acceleration of node H.
- Shear force, bending moment and axial force evaluated in the midpoint of the GE tube.
- Constraint force in C.

Specifically, the FRF has been calculated as:

$$\left(-\Omega^2\,[M_{FF}] + i\Omega\,[C_{FF}] + [K_{FF}]\right)\{X_0\} = \{F_0\} \tag{9}$$

where

$$[G\,(i\Omega)] = \left(-\Omega^2\,[M_{FF}] + i\Omega\,[C_{FF}] + [K_{FF}]\right)^{-1} \tag{10}$$

is the frequency response function matrix.

Since $\{Xo\}$ is computed for each Ω, we get a matrix of X_0 (not just a vector $ndof$ x 1) including all the DOFs of the system varying Ω. Thus, to monitor one single point of the response of the structure, we take the i-th row.

5.1. Vertical displacement and vertical acceleration of node F, horizontal displacement and horizontal acceleration of node H

The vertical displacement and vertical acceleration of node F and the horizontal displacement and horizontal acceleration of node H are illustrated below:

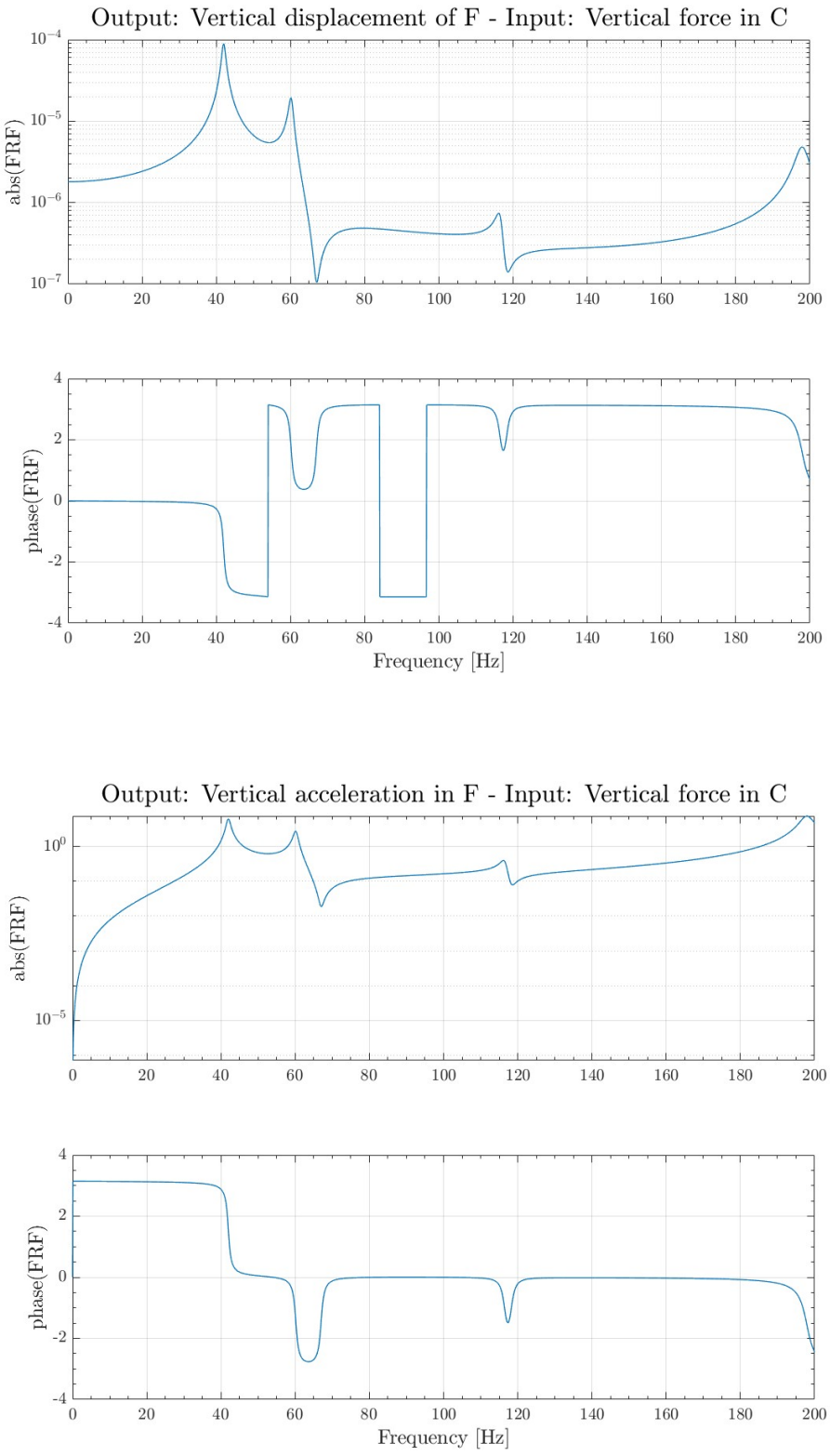

Figure 5: FRF relating the input force F_C to the displacements and accelerations of node F.

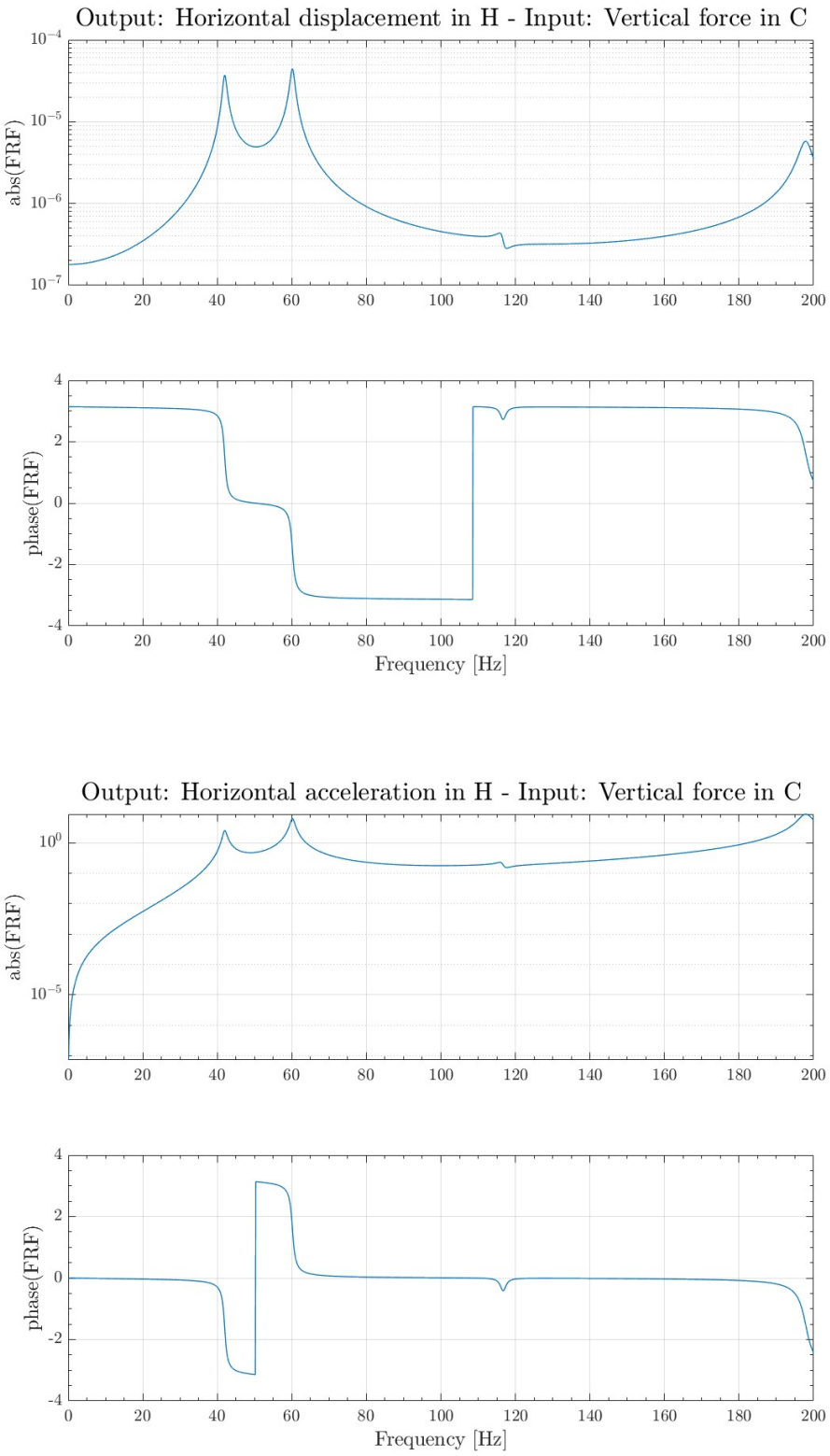

Figure 6: FRF relating the input force F_C to the displacement and acceleration of node H.

It can be noticed that the 4 resonance peaks are located exactly at the natural frequencies as it was expected, and consequently in correspondence of all the peaks, the phase is crossing $-\frac{\pi}{2}$. This means that the application of the force and then the location where we read the outputs along the bike frame, do not correspond with nodal positions.

For what concerns node H, it's possible to observe that the peak associated to mode 3 is much lower with respect to the others. Actually, analyzing the horizontal displacement of point H in that specific

mode (Figure 4) and comparing it with the others, this behaviour is justified.
The same can be said for node F where, also in this case, the peak of mode 3 is lower than the others. Looking at the vertical movement of this node in the aforementioned mode in figure 4, since it is limited, the FRF behaviour is justified.

Looking at the plots related to node F (Figure 5) an antiresonance is present: it corresponds to an almost null response of the system output, but it is not associated to a node of the structure.

Giving a look to the acceleration responses both for node F and H, at $f = 0Hz$, so in case of static force, the plot tends to 0: this is because the system is not vibrating. As a matter of fact, in the correspondent displacement plot the static displacement can be highlighted.

As a general comment, knowing the FRFs, it is important to come back to the natural frequencies and mode shapes information to give an interpretation of the response of the system.

5.2. Shear force, bending moment and axial force evaluated in the midpoint of the GE tube

According to the FE formulation, the axial and the transverse internal displacements of a beam section, respectively $u(\xi, t)$ and $w(\xi, t)$, are defined as functions of the nodal displacements ($\underline{x}$) through the shape functions ($\underline{f_u}$ and $\underline{f_w}$), which are defined in the local reference frame of each finite element.

In particular, the shape functions of the beam elements have a linear shape for the axial displacement and cubic for the transverse displacements, moreover enforcing the BCs for the beam element, its coefficients can be found as follows:

$$u(\xi, t) = a + b\xi \Rightarrow \begin{cases} a = x_i^L \\ b = \frac{x_j^L - x_i^L}{L_k} \end{cases} \tag{11}$$

$$w(\xi, t) = a + b\xi + c\xi^2 + d\xi^3 \Rightarrow \begin{cases} a = y_i^L \\ b = \theta_i^L \\ c = -\frac{3}{L_k^2} y_i^L + \frac{3}{L_k^2} y_j^L - \frac{2}{L_k} \theta_i^L - \frac{1}{L_k} \theta_j^L \\ d = \frac{2}{L_k^3} y_i^L - \frac{2}{L_k^3} y_j^L + \frac{1}{L_k^2} \theta_i^L + \frac{1}{L_k^2} \theta_j^L \end{cases} \tag{12}$$

Dealing with Euler-Bernoulli beam, the internal actions are computed:

$$N = EA\frac{\delta u}{\delta \xi}; \qquad M = EJ\frac{\delta^2 w}{\delta \xi^2}; \qquad T = EJ\frac{\delta^3 w}{\delta \xi^3}; \tag{13}$$

Note that, since $\epsilon_x = \frac{\delta u}{\delta \xi}$ is constant along the element length, then $\frac{\delta u}{\delta \xi} = b = \frac{x_j^L - x_i^L}{L_k}$. As a matter of fact, N is constant along the beam element. On the other hand, the bending moment and the shear force are proportional to the second and third partial derivatives of w with respect to ξ :

$$\begin{aligned} M = EJ\frac{\partial^2 w}{\partial \xi^2} \quad where \quad \frac{\partial^2 w}{\partial \xi^2} = 2c + 6d\xi; \\ T = EJ\frac{\partial^3 w}{\partial \xi^3} \quad where \quad \frac{\partial^3 w}{\partial \xi^3} = 6d \end{aligned} \tag{14}$$

Those partial derivatives can be rearranged in matrices allowing the writing of the internal forces as product of a vector, composed by the derivatives of the shape functions, and the nodal coordinates.

Therefore, the internal actions can be described with respect to the internal displacement field through the shape functions.

The following internal forces in the midpoint of GE tube (node 8) are obtained:

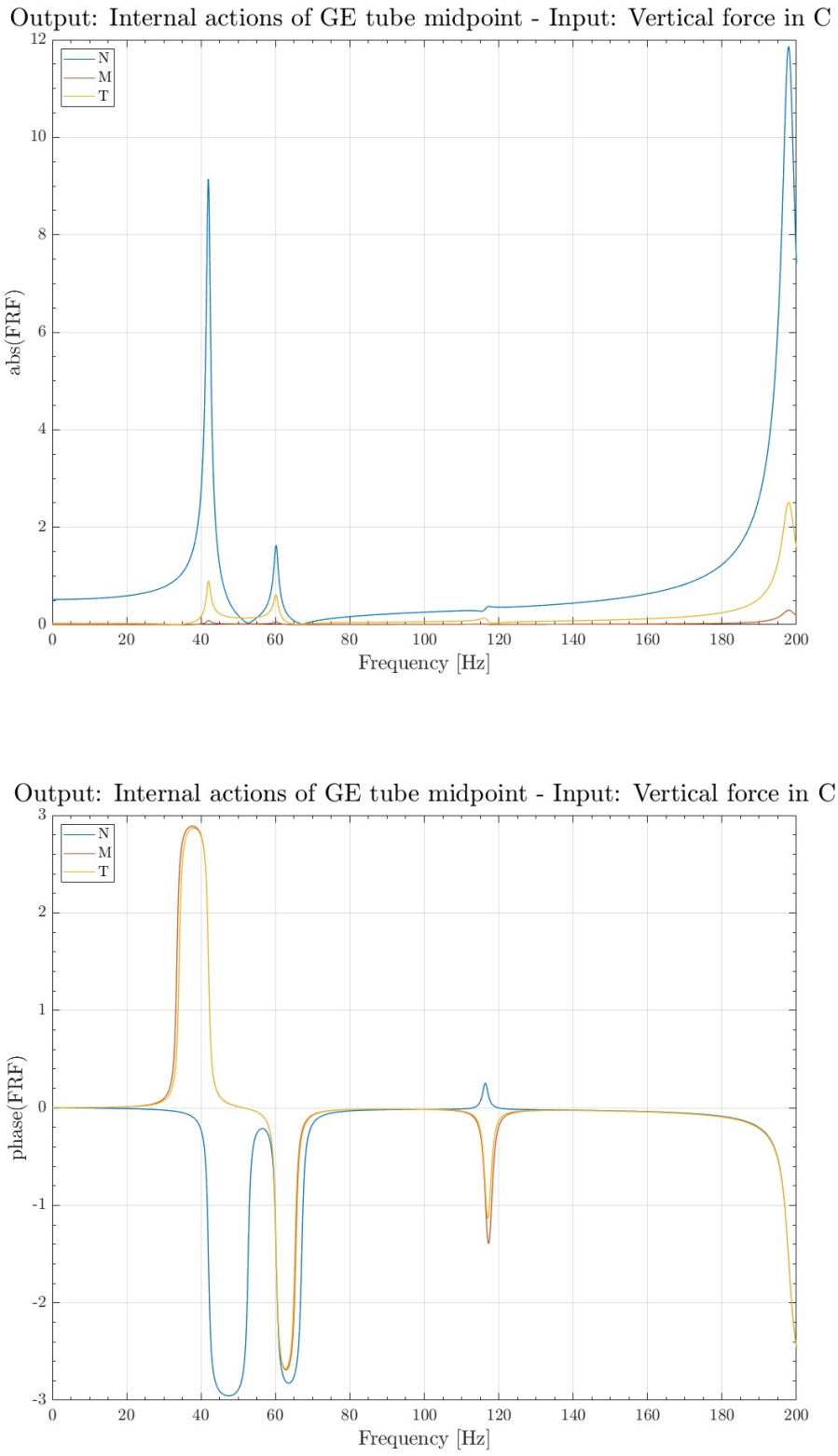

Figure 7: FRF relating the input force F_C to the internal actions in node I.

It is harder to understand the behaviour of the FRF related to the internal actions. All the resonance responses are correspondent to the position where we have the higher displacement, that is where we get higher internal actions. As a matter of fact, if T and M are related to the amount of displacement, the highest value of these derivatives are related to the highest value in terms of internal forces.

Since for the computation of the internal reaction forces it is needed to refer to the local coordinates, how the elements have been defined in the input file is crucial. As a matter of fact, in the present case in order to account for the GE element, a rotation matrix $[\Lambda]$ has been applied to the vector of the nodal displacements to switch from the global to the local reference frame (the actual system where this response of the system is described).

The last comment concerning the axial, shear and bending forces is related to the choice of the element in order to account for the node 8. It has been chosen the element 7 to compute the internal forces, but in case the element 6 was considered, we wont have obtained the same results: the shear forces are constant within the elements (this comes from the definition of the shape functions that allow us to obtain a constant shear force for the element, Equation 12). There is no solution concerning this, the shear force can just be considered as a piecewise function and the bending moment with a linear variation. The limitations of the shape functions are highlighted while computing the internal actions; higher is the mesh resolution, smaller is the approximation error introduced.

5.3. Constraint force in C

The constraint force can be computed as:

$$\{R\} = [M_{CF}]\{\ddot{x_F}\} + [C_{CF}]\{\dot{x_F}\} + [K_{CF}]\{x_F\} \tag{15}$$

knowing that: $\{x_F\} = \{X_0\}\, e^{i\Omega t}$ finally:

$$\{R\} = \left(-\Omega^2 [M_{CF}] + i\Omega [C_{CF}] + [K_{CF}]\right)^{-1} \{X_0\} \tag{16}$$

The correspondent plots are shown below:

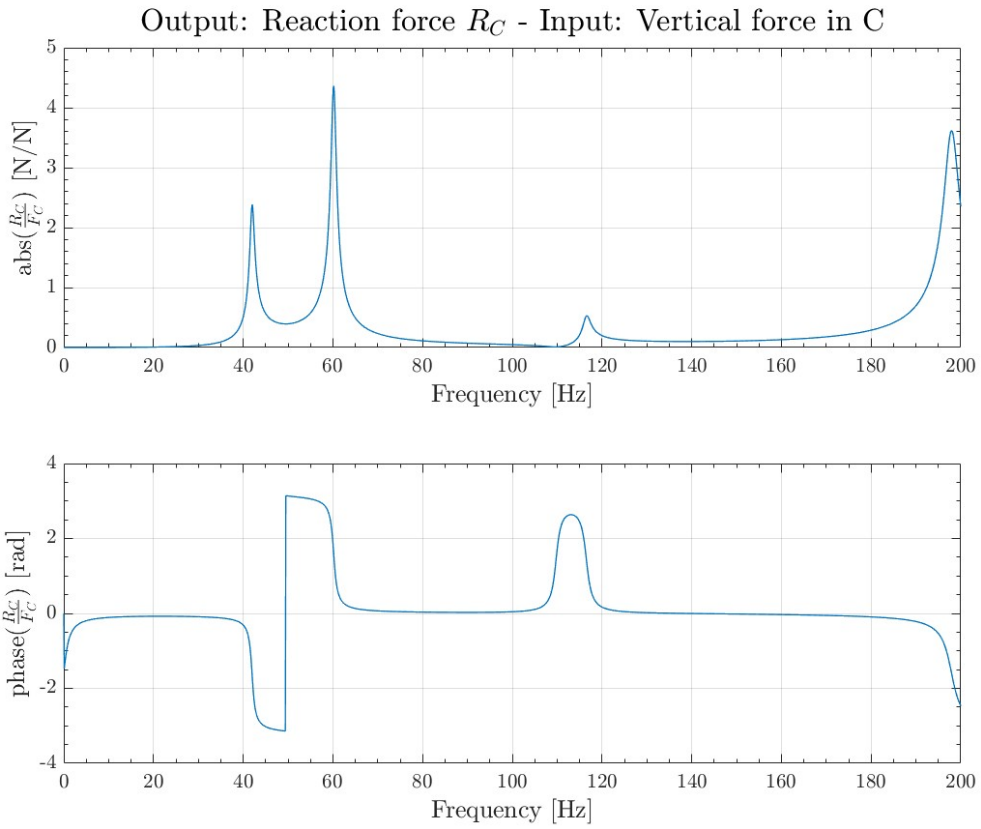

Figure 8: FRF relating the input force F_C to the horizontal reaction force in node C.

As expected, the FRF shows 4 peaks at the natural frequencies previously calculated.

5.4. Modal approach: Vertical displacement and vertical acceleration of node F, horizontal displacement and horizontal acceleration of node H

Despite the analysis of the structure staying in physical coordinates is feasible and gives reliable results being numerically computed, it is not possible to get an analytical quantitative description. Thus in order to completely understand the outputs of the FEM in terms of response functions of the system, the modal approach is needed. It exploits a linear transformation into the principal coordinates and it is extremely powerful since the complex behaviour of the structure is reduced to equivalent 1 DOF systems for a certain f range in the neighbour of each $\omega_{natural}$.

Relying on the modal approach, by which $\{\underline{x}(t)\} = [\Phi]\{\underline{q}(t)\}$ where $[\Phi] = \left[\{\underline{x}\}^{(1)}\{\underline{x}\}^{(2)}\cdots\{\underline{x}\}^{(n)}\right]$ is the transformation matrix (matrix of eigenvectors) and $\{\underline{q}(t)\}$ are the modal coordinates, it is possible to compute the modal mass, stiffness and damping matrices and the generalized force vector:

$$[M_q] = [\Phi]^T[M_{FF}][\Phi]; \quad [K_q] = [\Phi]^T[K_{FF}][\Phi]; \quad [C_q] = [\Phi]^T[C_{FF}][\Phi]; \quad [Q_q] = [\Phi]^T[F] \tag{17}$$

Thus, the equation of motion written in principal coordinates is:

$$[M_q]\{\ddot{q}\} + [C_q]\{\dot{q}\} + [K_q]\{q\} = \{Q_0\}e^{j\Omega t} \tag{18}$$

From this NDOF system, a set of N 1 DOF uncoupled equations is obtained:

$$m_{q,ii}\ddot{q}_i + c_{q,ii}\dot{q}_i + k_{q,ii}q_i = Q_{0i}e^{j\Omega t} \quad where \quad i = 1, 2, ..., n \tag{19}$$

In the case here presented n=2. Imposing $q_i = q_{0i}e^{j\Omega t}$:

$$q_{0i} = \frac{Q_{0i}}{(-\Omega^2 m_{q,ii} + j\Omega c_{q,ii} + k_{q,ii})} \tag{20}$$

As a result, the vertical displacement and acceleration of node F and the horizontal displacement and acceleration of node H (for the first 2 modes) are given by:

$$\{q_0\} = \frac{\{Q_0\}}{(-\Omega^2[M_q] + i\Omega[C_q] + [K_q])} \tag{21}$$

The correspondent plots are shown below:

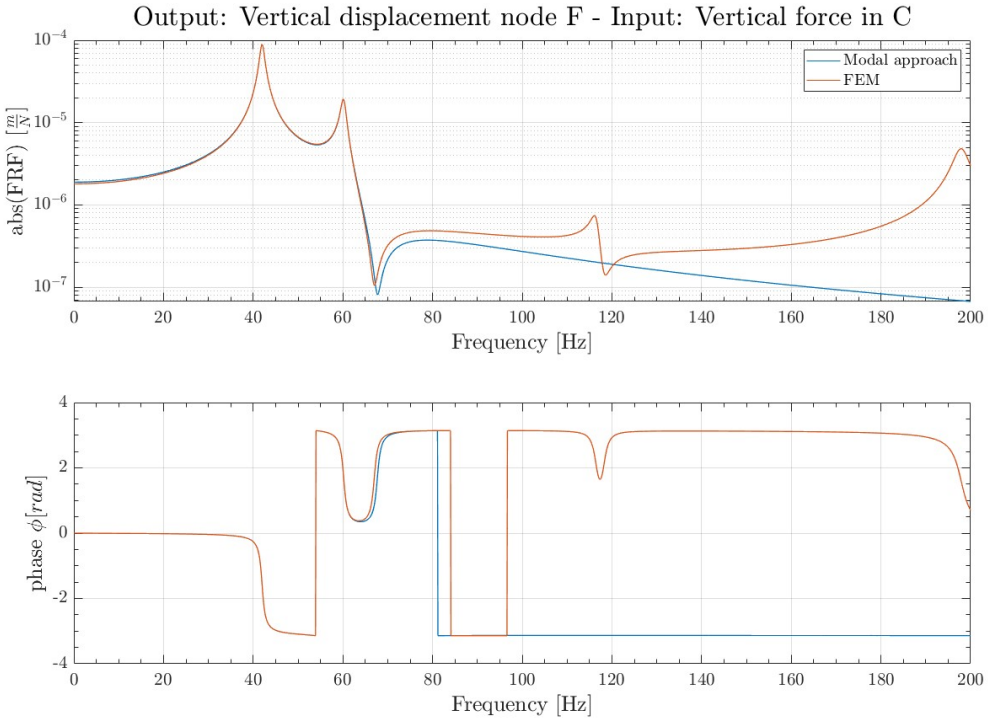

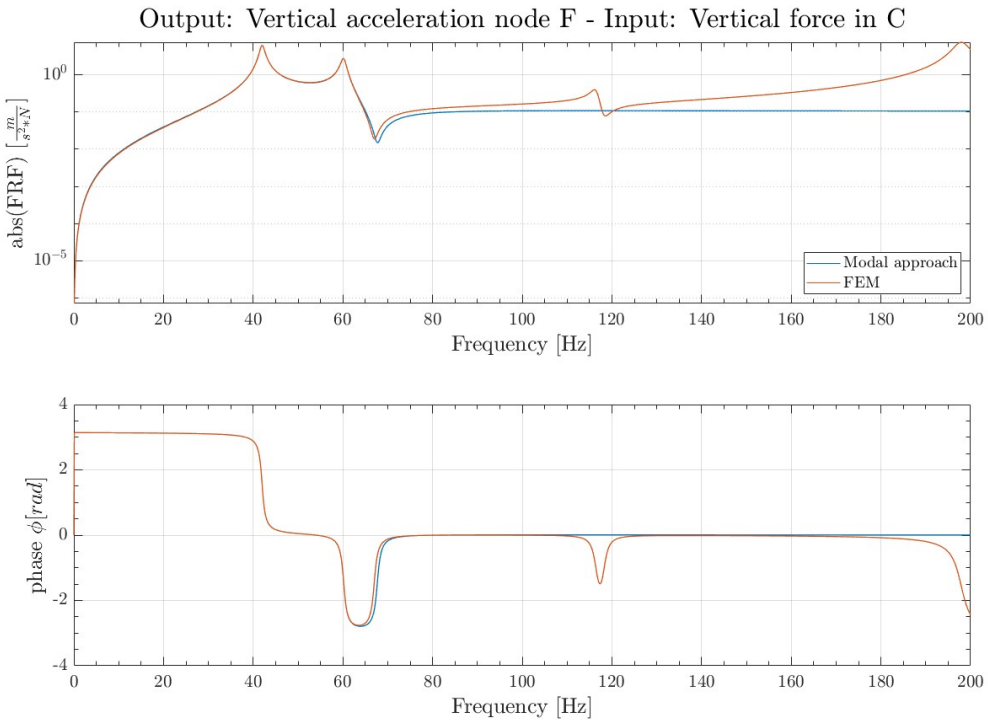

Figure 9: FRF relating the input force F_C to the displacements and accelerations of node F (Modal Approach VS FEM).

It's possible to assert that the FRF gives accurate results in the frequency range where the first 2 modes belong to: we have a perfect superposition of the 2 curves.The visible mismatch after the first 2 modes (f $>$ 60 Hz) is due to the fact that, in the FRF obtained thanks to the modal approach, only the first 2 modes are taken into consideration as stated above. Thus, increasing the number of modal contributions considered the mismatch would decrease. Also in the plots below this can be assessed.

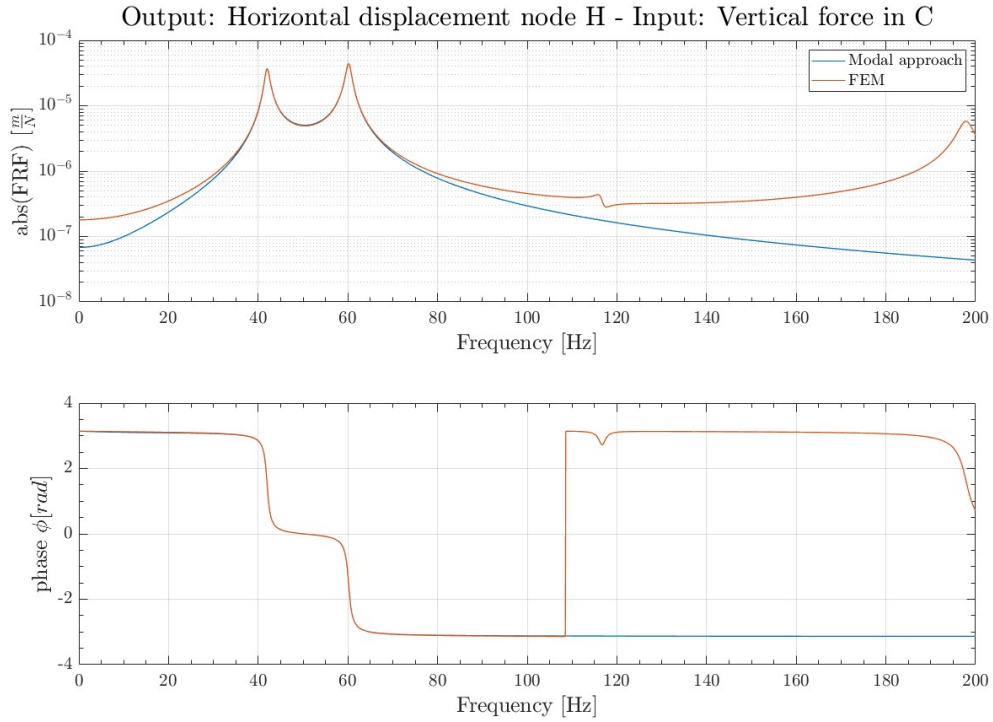

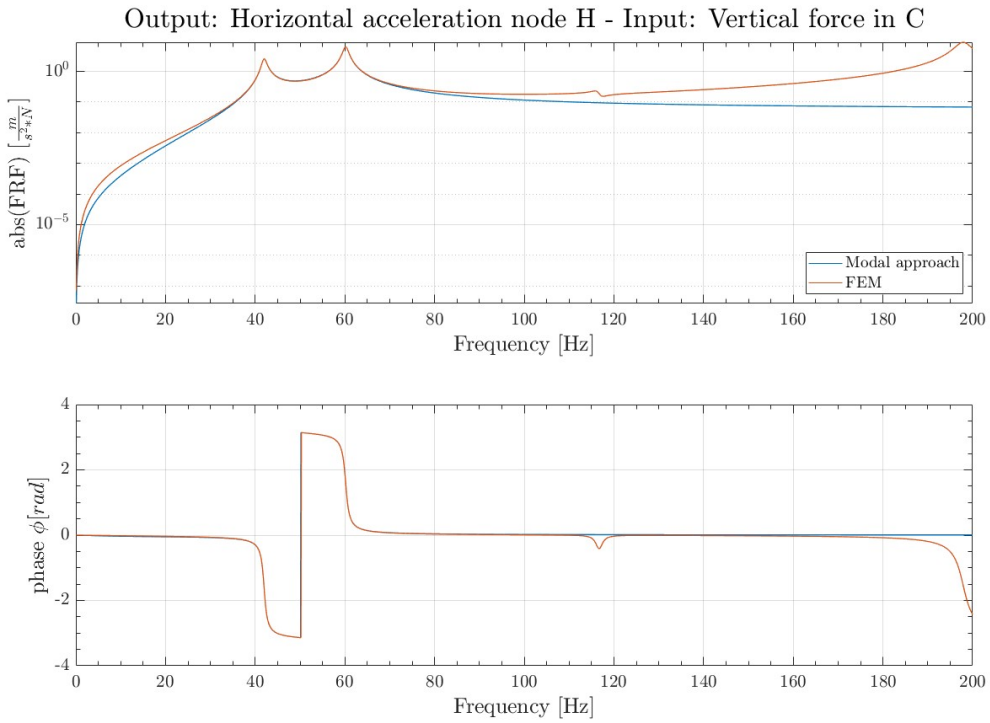

Figure 10: FRF relating the input force F_C to the displacements and accelerations of node H (Modal Approach VS FEM).

In Figure 10 a slight mismatch in the static response of the system is present. Actually, the static response is given by the sum of the static responses of all the modes and so, since the number of modes considered for the 2 curves is limited, a little discrepancy is straightforward. As a matter of fact, for the FRF related to displacement and acceleration of node H, it seems that the contribution to the static response of the first 2 modes is not enough. If the number of modes analyzed for the modal approach would have been higher, the divergence would have been minimized.

The use of the modal approach is useful and easier since:

- in the FEM the accuracy depends on the mesh adopted: if the mesh is not fair, the result will not be accurate;
- from a computational point of view in the modal approach we don't have to compute the inverse of full matrices as in the FEM (here we deal with scalars having diagonal matrices).

But, it is also true that the FEM has the advantage that is related to physical quantities, instead the principal coordinates do not have any physical meaning.

5.5. Input vertical displacement at point A' (ground imposed displacement) related to the output vertical acceleration at point F

In order to perform the calculation of the frequency response function relating the input vertical displacement of point A' (i.e. the bottom end of the front spring) to the output vertical acceleration at point F, it has been take into consideration node 1 and node 14 represented in figure 3 which are related to point A and point A' respectively. At this point the front spring is considered as an internal spring between the node placed on the frame and the one on the ground.

We are assuming that the constrained nodal vertical displacement of A' is defined through an harmonic function, therefore the FRF computation is:

$$\frac{\{x_0\}}{\{x_{C0}\}} = -\left\{-\Omega^2 M_{FF} + i\Omega C_{FF} + K_{FF}\right\}^{-1}\left\{-\Omega^2 M_{FC} + i\Omega C_{FC} + K_{FC}\right\} \tag{22}$$

In order to built the $\{\underline{xc}\}$ vector, we need to recall that in the global total configuration, all constrained nodal displacements are sorted in the last portion of the $\{\underline{x}_{GT}\}$.

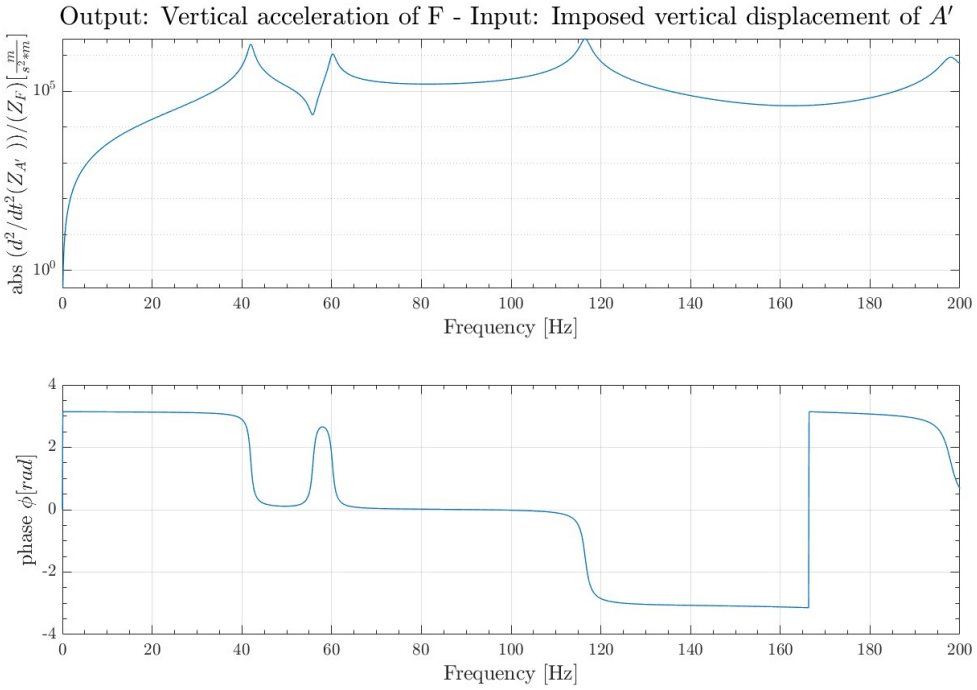

Figure 11: FRF relating the input force F_C to the ground imposed displacement of node A'.

As expected, the FRF shows 4 peaks at the natural frequencies previously calculated.

6. TIME HISTORY OF THE STEADY-STATE VERTICAL ACCELERATION OF POINT H

Knowing the expression of the FRF relating an input to the ground imposed displacement:

$$\frac{\{x_0\}}{\{x_{C0}\}} = -\left\{-\Omega^2 M_{FF} + i\Omega C_{FF} + K_{FF}\right\}^{-1}\left\{-\Omega^2 M_{FC} + i\Omega C_{FC} + K_{FC}\right\} \tag{23}$$

and that the bike travels with a speed of 12 $\frac{m}{s}$ on a sinusoidal road irregularity composed by two wavelengths λ_1 and λ_2 (of amplitude A_1, A_2 and phase φ_1, φ_2) hereafter reported (Table 2), it is possible to calculate the steady-state vertical acceleration of point H.

	$\lambda[m]$	$A[mm]$	φ	$f[Hz]$
1	1	1	0	12
2	0.6	0.5	0	20

Table 2: Properties of the road irregularity.

Computing the time response in steady state, it is needed to consider that the bike is travelling. This means that 2 different ground imposed displacement have to be considered both where the bike is connected to the ground (*node*15 wheel B and *node*14 wheel A). Thus, a phase delay between the first node and the second node is introduced: the wheel in point B is ahead the one in A, therefore their spatial variation has been taken into account introducing an anticipation in time for the signal of the wheel B. Obviously this is done for both wavelengths.

Furthermore, since it is asked to assume that at time $t = 0$ the centre of the front wheel (point A) is located above a positive maximum of the irregularity profile, a rigid translation for both wheel and both wavelength has been performed.

Below, the steady-state responses of the 2 wheels to λ_1 and λ_2 have been considered separately (Figure 12) and then together thanks to the superimposition principle (Figure 13):

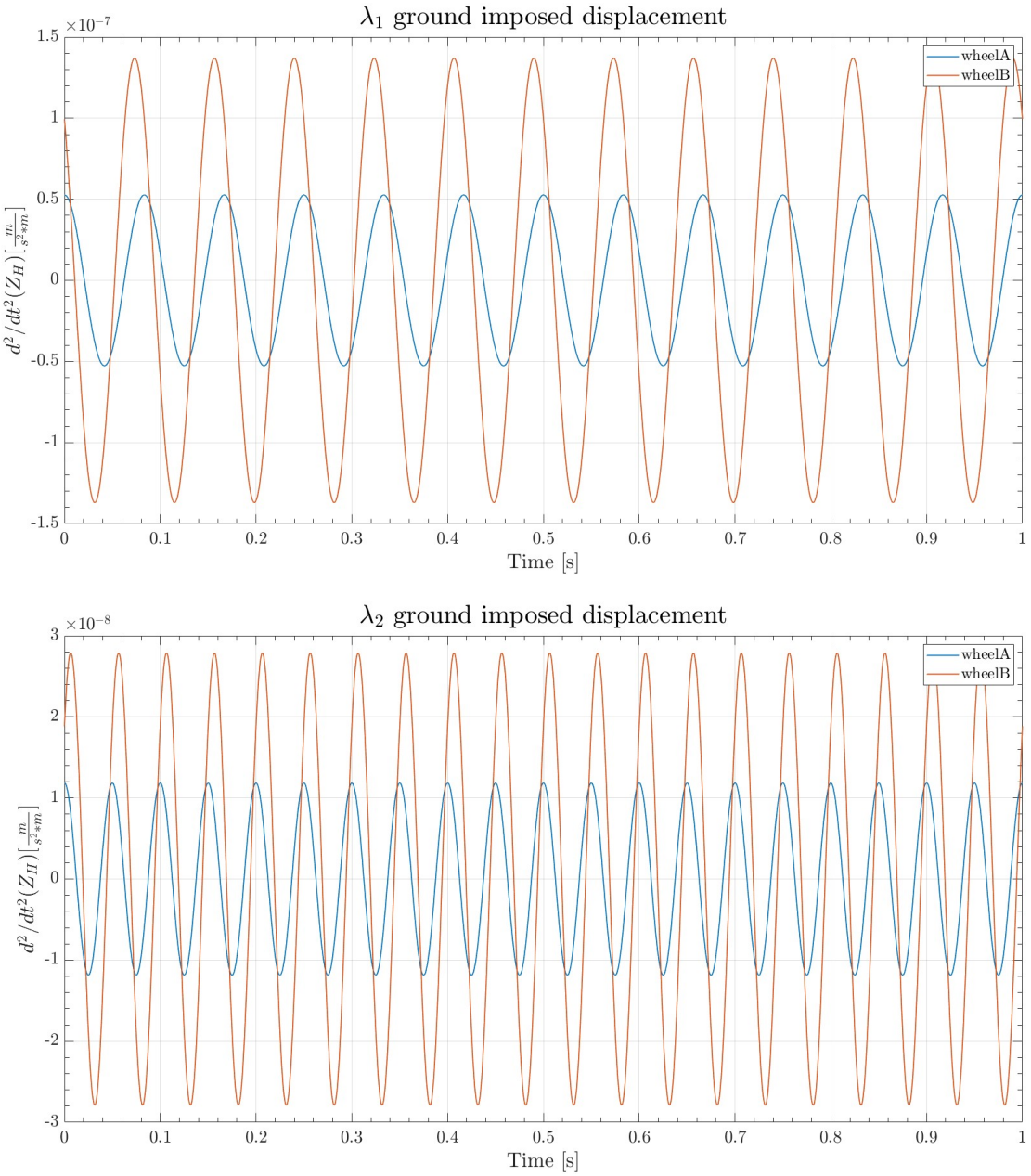

Figure 12: Steady-state vertical acceleration of point H (saddler) due to the bike motion on a irregular road.

Note that, the part of the solution associated to the homogeneous problem of the ordinary differential equation (ODE) vanishes in time due to damping, so that the steady state response is just described by what is computed through the FRF. This is why starting from the FRF, it is just matter to select one value of Ω (related to the external force or ground imposed displacement chosen) switching back in time domain.

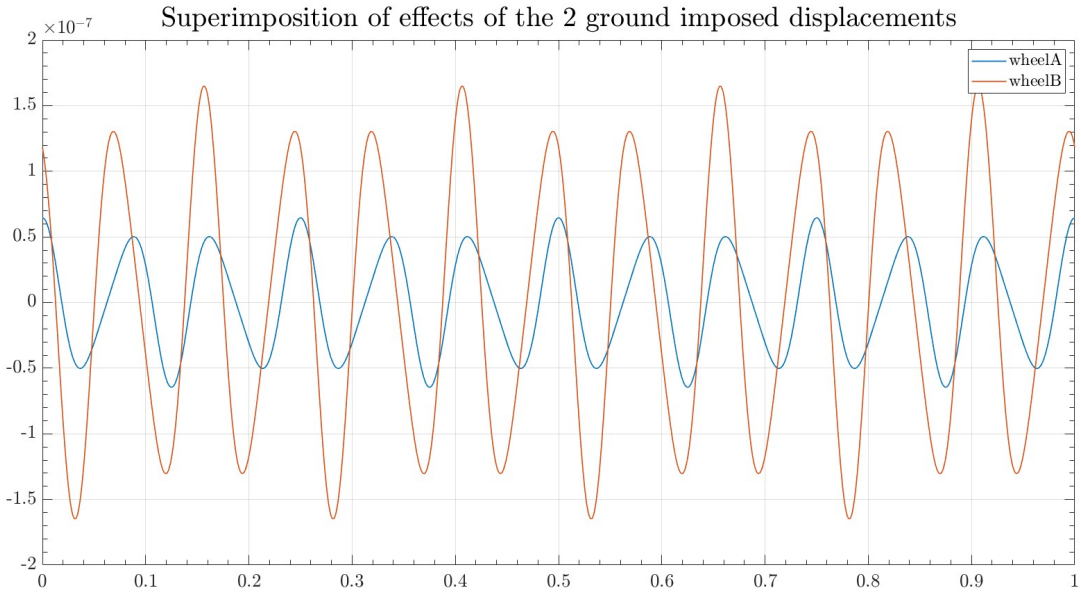

Figure 13: Steady-state vertical acceleration of point H (saddler) due to the bike motion considering both $\lambda 1$ and $\lambda 2$

7. STATIC RESPONSE OF THE STRUCTURE DUE TO THE CYCLIST WEIGHT

The aim of this last analysis is the computation of the static deflection of the bike frame due to the weight of the cyclist, which is represented by $P_H = -600N$ vertical force applied in H (the saddle) plus $P_F = -100N$ vertical force applied in F (the handlebar).
Note that the forces have been considered with a minus sign since their verse is opposite to the reference axis one.

The general free nodal coordinates equation of motion is:

$$[M_{FF}]\{\ddot{x}_F\} + [C_{FF}]\{\dot{x}_F\} + [K_{FF}]\{x_F\} = \{F_0\} \tag{24}$$

The static deflection of the structure is computed accounting only for constant forces and potential energy derivatives (i.e. generalized components of constant conservative forces). Therefore, in static conditions are considered $\{\ddot{x}_F\} = 0$ and $\{\dot{x}_F\} = 0$, so that:

$$\{x_F\} = [K_{FF}]^{-1}\{F_0\} \tag{25}$$

where vector $\{x_F\}$ contains all the actual nodal displacements due to the forces F_0 in the global reference frame with respect to the reference condition

Here below the system static deflection is represented along with an indication (black arrow) of the vertical displacement of node 8 (midpoint of the GE tube):

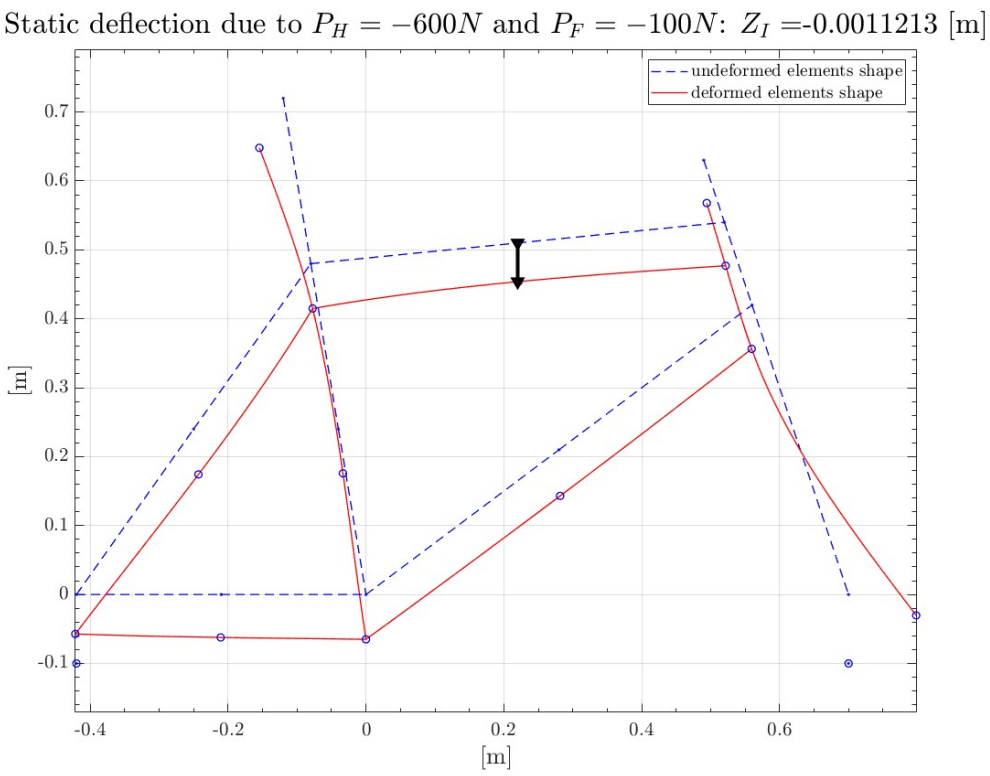

Figure 14: Static deflection of the system due to the weight of the cyclist

It is important to notice that a magnification coefficient $MC = 50$ has been included in Figure 14 to better appreciate the static response of the bike frame. This is why the actual value $Z_I = 1.1213mm$ is not consistent with the actual deformed shape representation.